

TRIGGERING AND DELIVERY ALGORITHMS FOR AGN FEEDBACK

GREGORY R. MEECE^{1,2}, G. MARK VOIT¹, BRIAN W. O'SHEA^{1,3,4,5}

Draft version September 29, 2018

ABSTRACT

We compare several common sub-grid implementations of AGN feedback, focusing on the effects of different triggering mechanisms and the differences between thermal and kinetic feedback. Our main result is that pure thermal feedback that is centrally injected behaves differently from feedback with even a small kinetic component. Specifically, pure thermal feedback results in excessive condensation and smothering of the AGN by cold gas because the feedback energy does not propagate to large enough radii. We do not see large differences between implementations of different triggering mechanisms, as long as the spatial resolution is sufficiently high, probably because all of the implementations tested here trigger strong AGN feedback under similar conditions. In order to assess the role of resolution, we vary the size of the “accretion zone” in which properties are measured to determine the AGN accretion rate and resulting feedback power. We find that a larger accretion zone results in steadier jets but can also allow too much cold-gas condensation in simulations with a Bondi-like triggering algorithm. We also vary the opening angle of jet precession and find that a larger precession angle causes more of the jet energy to thermalize closer to the AGN, thereby producing results similar to pure thermal feedback. Our simulations confirm that AGN can regulate the thermal state of cool-core galaxy clusters and maintain the core in a state that is marginally susceptible to thermal instability and precipitation.

1. INTRODUCTION

An active galactic nucleus (AGN) is thought to be present in the core of nearly every massive galaxy and galaxy cluster. Based on estimates of jet power from AGN-inflated cavities, it has become clear that an AGN can strongly influence cooling and condensation of gas in its host galaxy (e.g., [McNamara & Nulsen 2012](#)), potentially explaining the relationships observed between the mass of a galaxy’s central black hole and the velocity dispersion of its stars (e.g., [Merritt 2000](#); [Ferrarese & Merritt 2000](#)), as well as the star-formation properties of galaxies with AGNs (e.g., [Kauffmann et al. 2003](#)). Directly simulating the co-evolution of AGNs together with their host galaxies is not computationally feasible due to the large differences in mass and size between an AGN and its host galaxy. Also, the diverse set of complex physical processes that govern AGN accretion and outflow production remain poorly understood. To circumvent these difficulties in studies of galaxy evolution, simulators have developed a number of “subgrid” implementations of AGN feedback that are intended to capture the interplay between the AGN and its environment without representing the details of AGN accretion on smaller scales (see, for example [Omma et al. 2004](#); [Springel et al. 2005a](#); [Puchwein et al. 2008](#); [Booth & Schaye 2009](#); [Gaspari et al. 2011b](#); [Dubois et al. 2012](#); [Li & Bryan 2014a](#); [Steinborn et al. 2015](#)). However, subgrid implementations of AGN feedback vary widely, and there has been little systematic comparison (but see [Wurster & Thacker 2013](#); [Yang et al. 2012](#)). From the explorations of parameter space carried out in these studies, it has become evident that varying certain AGN feedback parameters can lead to strong dif-

ferences in feedback power and energy propagation. In this paper, we compare several of the popular methods for implementing AGN feedback.

An AGN consists of a supermassive black hole (SMBH) surrounded by a disk of accreting material. Twisted magnetic fields in the disk are thought to channel charged particles into jets, which can draw additional power from the spin of the SMBH via the Blandford-Znajek effect ([Blandford & Znajek 1977](#); [Blandford & Payne 1982](#)). These relativistic jets produce synchrotron emission, which is observed in the radio band. Hence, this mode of AGN energy output is termed “radio-mode” feedback (e.g., [Churazov et al. 2001](#); [Springel et al. 2005b](#)). Additionally, differential rotation in the accretion disk will heat the accreting material, producing a strong UV flux. If the SMBH is accreting near the Eddington Limit, radiation pressure may also drive large outflows. This “quasar-mode” feedback (e.g., [Churazov et al. 2005](#)) is composed of non-relativistic material and is more isotropic than radio-mode feedback.

The length and mass scales that are important for AGN are much smaller than the range covered by galaxies and galaxy clusters. For example, a black hole with a mass similar to the one dwelling at the center of the Perseus Cluster ($\sim 3.4 \times 10^8 M_{\odot}$; see [Wilman et al. 2005](#)) has a Schwarzschild radius of only a few AU, whereas the virial radius of a galaxy cluster is $\gtrsim 1$ Mpc. Cosmological simulations capable of modeling entire galaxy clusters typically have a maximum resolution of ~ 1 kpc, meaning that the AGN’s behavior must be approximated with a subgrid model. Furthermore, AGN are known to be variable on timescales much shorter than the dynamical time of a galaxy. Cosmological simulations that model structure formation over a Hubble Time must therefore rely on an AGN model that smooths out this short-term variability while preserving the large-scale behavior of the resulting feedback.

In order for a self-regulated feedback loop to arise, a sub-grid AGN model must capture the coupling between an AGN and its fuel supply. A triggering algorithm must somehow

¹ Department of Physics and Astronomy, Michigan State University, East Lansing, MI 48824

² Corresponding author: meecegre@msu.edu

³ Department of Computational Mathematics, Science and Engineering, Michigan State University, East Lansing, MI 48824

⁴ National Superconducting Cyclotron Laboratory, Michigan State University, East Lansing, MI 48824

⁵ Lyman Briggs College, Michigan State University, East Lansing, MI 48825

estimate the mass accretion rate onto the SMBH, which translates into a proportional release of feedback energy. Then a delivery algorithm must prescribe how that feedback energy interacts with the local environment. In cosmological simulations, the subgrid AGN model must also include prescriptions for following the creation, advection, and merger of SMBHs, although these are not discussed in this work (see [Sijacki et al. 2007](#); [Di Matteo et al. 2008](#); [Wurster & Thacker 2013](#); [Vogelsberger et al. 2013](#), for more discussion on these topics). Instead, we are focusing on just the triggering and delivery algorithms.

There are a number of reasons to believe that AGN feedback in massive galaxies is self-regulated. First, as stated earlier, strong relationships have been found between the masses of SMBHs and the properties of their host galaxies. Second, AGNs are considered the best candidates for solving the “Cooling Flow” problem in galaxy clusters and elliptical galaxies ([Binney & Tabor 1995](#); [McNamara & Nulsen 2007](#); [Nulsen & McNamara 2013](#)). Many galaxy clusters have central cooling times that are far shorter than the age of the clusters, but the observed star-formation rates are an order of magnitude or more below what would be expected from uninhibited cooling ([O’Dea et al. 2008, 2010](#); [McDonald et al. 2011](#)). Also, the amounts of cold gas that seem to be accumulating are much less than one would naively expect ([Peterson et al. 2003](#); [Peterson & Fabian 2006](#)). This tension implies the existence of a heat source that roughly balances cooling losses. Non-AGN heat sources, such as supernovae, mergers, conduction, and preheating have been proposed, but are either not powerful enough to balance cooling (e.g., [Skory et al. 2013](#)) or are inconsistent with observations. AGNs, however, are known to be present in the central galaxies of galaxy clusters and produce feedback energy comparable to the cooling rate. [Binney & Tabor \(1995\)](#) showed that when cooling-triggered jets are added to models of cool-core clusters, alternating periods cooling and jet heating can lead to a quasi-steady state for the ICM in the cluster core. As discussed in [McNamara & Nulsen \(2012\)](#), the jet power must be closely coupled to the cooling rate if AGN are balancing cooling in clusters. Otherwise, the AGN would either overheat or underheat the intra-cluster medium (ICM).

One simple algorithm for estimating the AGN accretion rate bases the scaling properties on the Bondi-Hoyle accretion model, set out in [Bondi \(1952\)](#), which implicitly assumes that the SMBH is accreting hot ambient gas directly from the ICM. Strictly speaking, such a Bondi accretion flow should be steady-state, spherically symmetric, and isentropic. Accretion then becomes supersonic within the Bondi radius given by $R_{\text{Bondi}} \approx 2GM_{\text{BH}}/c_s^2$ where M_{BH} is the black hole mass and c_s is the sound speed of the gas near R_{Bondi} , and proceeds at a rate \dot{M}_{Bondi} that depends on M_{BH} and c_s . However, the Bondi radius is unresolved in many numerical simulations of AGN feedback, as is its impact on galaxy evolution. [Springel et al. \(2005a\)](#) therefore proposed a parameterized Bondi accretion rate with an artificial boost factor α such that $\dot{M}_{\text{BH}} = \alpha \dot{M}_{\text{Bondi}}$. The boost factor α is typically chosen to be large because the actual gas properties at the Bondi radius are likely to permit a greater accretion rate than would arise in under-resolved simulations. [Springel et al. \(2005a\)](#) and subsequent studies following up on that work use $\alpha = 100$, while [Khalatyan et al. \(2008\)](#) use $\alpha = 300$. [Hopkins & Hernquist \(2006\)](#), in contrast, use a factor that is near unity, albeit for studies of galaxy-scale phenomena.

In reality, the assumptions of Bondi accretion — steady homogeneous flow, spherical symmetry, and adiabaticity — are unlikely to be valid near the Bondi radius around a massive galaxy’s SMBH (see, for example, the discussion in [Mathews & Guo 2012](#)). Furthermore, models relying on standard Bondi accretion have problems generating sufficiently powerful outflows without a large boosting factor (see BS09 for discussion) and with reproducing the properties of observed cool-core clusters absent fine tuning. An alternative model for self-regulated accretion, described by [Pizzolato & Soker \(2005\)](#), posits that the AGN is primarily fueled by accretion of cold, dense gas that rains down in a stochastic manner. Aside from the prior assumption that the AGN heating rate is linked to cooling in the ICM, this model is supported by observations of cold gas and star formation which indicate that at least some gas is able to cool (e.g., [Edge 2001](#); [Cavagnolo et al. 2008](#); [O’Dea et al. 2008](#)). In this “moderate cooling flow” or “cold feedback” model, radial mixing resulting from strong AGN outbursts creates large inhomogeneities that cool and condense at radii between 5 and 30 kpc from the AGN. The condensates then rain down on the SMBH, powering subsequent outbursts. This model couples the AGN to the cooling properties of the entire cluster core rather than only to the region directly surrounding the SMBH. Importantly, the coupling also occurs over timescales longer than the freefall in the core, leaving time for gas to cool and condense. Cold mode feedback has been implemented in recent simulations, notably those of [Gaspari et al. \(2011a,b, 2012\)](#); [Li & Bryan \(2014a,b\)](#); [Li et al. \(2015\)](#), which attain self-regulated states similar to those observed in galaxy-cluster cores.

To mimic the effects of both cold and hot accretion modes, [Booth & Schaye \(2009\)](#), hereafter referred to as BS09) proposed a model that invokes Bondi accretion with a density-dependent boost factor. This boost factor equals unity at low densities, giving the classical Bondi accretion rate, but ramps up quickly above a pre-chosen density threshold in order to account, rather crudely, for cooling, condensation, and accretion of condensed gas.

In the simplest models for delivery of AGN feedback, all of the feedback energy is assumed to thermalize at scales below the resolution of the grid and is deposited as thermal energy in a small central region. This approach is used in [Springel et al. \(2005a\)](#) and subsequent works, including recent simulations such as the Illustris simulation ([Vogelsberger et al. 2014](#)), Rhapsody-G ([Hahn et al. 2015](#)) and the simulations of [Rasia et al. \(2015\)](#). In reality, AGN outflows are likely asymmetric on scales of several kpc with a significant proportion of their energy in kinetic form. Such bipolar outflows may be important for transporting feedback energy to large distances from the AGN and for mixing metals out to distances of ~ 100 kpc from the central galaxy ([Kirkpatrick et al. 2011](#); [Kirkpatrick & McNamara 2015](#)). Although much work has been done studying highly collimated outflows on small scales over short time periods ([Vernaleo & Reynolds 2006](#); [Omma et al. 2004](#)), it is not straightforward to implement them in large-scale simulations with coarser resolution.

Given the increasing awareness that a proper treatment of AGN feedback is essential for accurate modeling of the evolution of large galaxies, it is important that the consequences of different AGN feedback implementations be understood. The rest of this paper compares several commonly used algorithms for triggering and delivery of AGN feedback in the context of an idealized galaxy-cluster core, in order to explore

how they differ in representing the coupling of an AGN to its environment, the total AGN feedback energy produced, and the resulting thermodynamic profiles of the ambient medium. Section 2 discusses our simulation setup and outlines the triggering and delivery methods we study. Section 3 describes the results of changing the triggering and delivery algorithms. Section 4 discusses our results in the context of thermal-instability analyses of cold gas accumulation and self-regulation, along with a discussion of how physical processes that were not included might have affected our results if they had been included. Finally, Section 5 summarizes the key results and points out avenues and opportunities for further study.

2. METHOD

In this work, we consider the interplay between ICM cooling and AGN feedback using a simplified AGN model in an idealized galaxy cluster environment. The simulations are performed using the adaptive mesh hydrodynamics code Enzo⁶ (Bryan et al. 2014) and analyzed using the yt⁷ analysis toolkit (Turk et al. 2011).

2.1. Simulation Environment

Our simulations include hydrodynamics, gravity, radiative cooling, and AGN feedback. We use a static gravitational potential representing both the cluster and its BCG but do not account for the self-gravity of the gas, which we assume to be negligible. We use a tabulated cooling function taken from Schure et al. (2009), assuming a uniform metallicity of half the Solar value. This cooling function does not allow gas to cool below 10^4 K, which does not affect the qualitative behavior of our simulations, since any processes occurring at lower temperatures would take place below our spatial resolution limit. For analysis purposes, we define any gas below 3×10^4 K as “cold.” Section 4.2 discusses the potential effects of including additional physical processes such as magnetic fields, conduction, and star formation, which may affect AGN feedback but are not included in our simulations.

Unless otherwise noted, the simulation setup encompassed a box of length 3.2 Mpc per side with a 64^3 cell root grid and 8 levels of AMR refinement, giving a maximum spatial resolution of 196 pc. A set of 8 nested grids, centered on the cluster core, with twice the resolution and half the width of the previous level, were created during initialization and were never de-refined. Additional refinement was allowed to occur based on strong density or energy gradients, baryon overdensity, and cooling. All cells containing material that was ejected from the central 10 kpc, as indicated by a passive tracer field added to material within that region, were covered by at least 4 levels of refinement. Finally, the zone around the AGN where accretion was measured and feedback was applied was always refined to the maximum level. We do not take cosmological expansion into account.

2.2. Cluster Setup

Following the work of Li & Bryan (2012), we initialize the ICM as a hydrostatic sphere of gas within a static spherical gravitational potential. The gravitational potential comprises two components: an NFW halo and the stellar mass profile of the BCG. The virial mass M_{200} and concentration parameter c of the NFW halo are defined with respect to the radius within

which the mean mass density is 200 times the critical density. For the BCG we assume a mass profile of the form

$$M_*(r) = M_4 \left[\frac{2^{-\beta_*}}{(r/4\text{kpc})^{-\alpha_*} (1+r/4\text{kpc})^{\beta_*-\alpha_*}} \right], \quad (1)$$

where M_4 is the stellar mass within 4 kpc and α_* and β_* are constants. As in Li & Bryan (2012) and Mathews et al. (2006), we used the Perseus cluster as a template, choosing $M_{200} = 8.5 \times 10^{14} M_\odot$, $c = 6.81$ for the NFW halo, $M_4 = 7.5 \times 10^{10} M_\odot$, $\alpha_* = 0.1$, and $\beta_* = 1.43$ for the BCG. With these mass profiles, the BCG is gravitationally dominant $\lesssim 10$ kpc from the center, while outside of this radius the NFW halo dominates the potential.

Although we do not take cosmological expansion into account in our simulations, we do use a vanilla Λ CDM model in order to specify the virial mass of the NFW halo and to set its gas temperature. For initialization, we assume a cluster at redshift $z = 0$ and a cosmology with $\Omega_M = 0.3$, $\Omega_\Lambda = 0.7$, and $H_0 = 70$ km/s/Mpc. We do not expect our results to be sensitive to small changes in these parameter values.

The hydrostatic gas in the halo is initialized with an entropy profile of the form

$$K(r) = K_0 + K_{100}(r/100\text{kpc})^{\alpha_K} \quad (2)$$

where we use the definition of specific entropy used in the ACCEPT database (Cavagnolo et al. 2009):

$$K \equiv \frac{k_B T}{n_e^{2/3}}. \quad (3)$$

For the Perseus cluster, ACCEPT gives values of $K_0 = 19.38$ keV cm², $K_{100} = 119.87$ keV cm², and $\alpha_K = 1.74$, and we use them for our initial configuration. The condition for hydrostatic equilibrium is

$$\frac{dP}{dr} = -\rho g. \quad (4)$$

Together, the the specified entropy profile and the hydrostatic condition (equations 2, 3, and 4) give a differential equation relating temperature and entropy. It remains to specify a boundary condition so that this equation can be integrated. Following Voit (2005), the temperature of a hydrostatic ICM can be approximated as

$$k_B T_{200} = \frac{\mu m_p}{2} [10GM_{200}H(z)]^{2/3} \quad (5)$$

We take this as a characteristic temperature for the ICM near the virial radius and integrate inwards and outwards to find the temperature and density profiles for the rest of the cluster.

2.2.1. Tracer Fluid

In order to track the gas directly affected by AGN feedback, we continuously inject a (passive) tracer fluid into the central 10 kpc. This passive tracer also allows us to measure the radial extent of feedback heating and also indicates the amount of metal transport facilitated by AGN jets and rising cavities, which are thought to play an important role in shaping the metallicity profiles of clusters. The amount of tracer injected per unit mass $\Delta\rho_T$ is given by

$$\Delta\rho_T = \text{SSFR} * Y \quad (6)$$

where we assume a specific star-formation rate $\text{SSFR} = 10^{-11}$ yr⁻¹ and a yield $Y = 0.02$. These assumptions are meant to be

⁶ <http://enzo-project.org/>

⁷ <http://yt-project.org/>

a crude approximation for metal injection by the old stellar population of the BCG. We emphasize that all we are doing is injecting passive tracer fluid. No actual star formation takes place, and the tracer fluid does not affect the radiative cooling rate. Our primary interest is radial transport and distribution of the tracer fluid. We do not expect its concentration to match metallicity values in the ICM of observed clusters.

2.3. Feedback and Jet Modeling

AGN are complicated systems governed by physical processes that are poorly constrained and span many orders of magnitude in space and time. Our goal here is not to understand all the details of AGN physics but rather to study the interplay between accretion, jet outflows, and the thermal state of the ICM. To this end, we implement a simplified ‘‘AGN Particle’’ model, wherein accretion onto the AGN launches outflows that are insensitive to the details of gas accretion on scales < 200 pc. We implement several triggering mechanisms, each with a different algorithm for determining the accretion rate \dot{M} into the region surrounding the central supermassive black hole, which sets the scale of the AGN feedback response. In each case, the resulting output of feedback power is taken to be $\dot{E} = \epsilon \dot{M} c^2$, where ϵ is a feedback efficiency factor and c is the speed of light. The accretion rate \dot{M} is not necessarily the actual accretion rate onto the central black hole, and in our idealized implementations no gas is removed from the simulation volume. Instead, it is assumed to be reheated and expelled from the vicinity of the black hole by feedback. Regardless of the triggering mechanism, precessing jets are launched from disk-shaped regions on either side of the AGN as described in the following subsections. Please refer to Table 1 for fiducial values of the AGN feedback parameters.

2.3.1. Triggering Mechanisms

Each of the following triggering methods calculates \dot{M} and removes gas mass from the grid within a specified radius given by the parameter R_{acc} .

Cold-Gas Triggered Feedback — Meant to replicate the triggering mechanism used in Li & Bryan (2014a), feedback is triggered by the presence of gas within R_{acc} and at or below a threshold temperature T_{floor} . The accretion rate corresponding to a single cell is

$$\dot{M}_{\text{cell}} = \frac{M_{\text{cell}}}{t_{\text{acc}}} \quad (7)$$

where t_{acc} is a constant timescale. Following Li & Bryan (2014a), we choose $t_{\text{acc}} = 5\text{Myr}$, which is close to the average freefall time near the accretion radius.

Boosted Bondi-like Triggering — The accretion rate is set to the Bondi accretion rate derived from conditions within R_{acc} and multiplied by a constant boost factor α so that

$$\dot{M} = \alpha \frac{2\pi G^2 M_{\text{BH}}^2 \hat{\rho}}{(\hat{v}^2 + \hat{c}_s^2)^{3/2}} \quad (8)$$

where G is the gravitational constant, M_{BH} is the mass of the black hole, and $\hat{\rho}$, \hat{v} , and \hat{c}_s are the mass-averaged density, velocity magnitude, and sound speed within R_{acc} . In this work we adopt $\alpha = 100$. Mass is removed from each cell within R_{acc} in a mass-averaged sense, such that

$$\Delta M_{\text{cell}} = \frac{M_{\text{cell}}}{M(< R_{\text{acc}})} \dot{M} \Delta t \quad (9)$$

Table 1
Fiducial AGN Feedback Parameters

| Parameter | Value | Description |
|---------------------|-----------------------------|-----------------------------------|
| ϵ | 10^{-3} | Jet efficiency |
| R_{acc} | 0.5 kpc | Accretion radius |
| T_{Floor} | 3×10^4 K | Temperature floor |
| M_{BH} | $1.0 \times 10^8 M_{\odot}$ | SMBH mass |
| ϕ_{Jet} | 0.15 radians | Jet precession angle |
| τ_{Jet} | 10 myr | Jet precession period |
| R_J | 0.5 kpc | Radius at which jets are launched |
| R_D | 0.5 kpc | Initial radial thickness of jets |

Note. — These parameter values are used for all simulations unless otherwise noted in the text.

Booth and Schaye Accretion — As described in BS09, the accretion rate follows the Bondi formula but with a boost that depends on the gas density as

$$\alpha = \begin{cases} 1 & n \leq n_0 \\ (n/n_0)^\beta & n > n_0 \end{cases} \quad (10)$$

Following Booth & Schaye (2009), we take $n_0 = 0.1 \text{ cm}^{-3}$ and $\beta = 2$.

2.3.2. Jet Implementation

After the total accretion rate \dot{M} during a timestep Δt is calculated with one of these triggering methods, a corresponding amount of feedback energy $\epsilon \dot{M} c^2 \Delta t$ is added to the ejected gas. We assume the ejected mass to be equal to $\dot{M} \Delta t$, which is an idealization. In reality, the mass-loading factor of the jets will depend on subgrid physics that is not yet well understood. However, Dubois et al. (2012) find that the choice of mass-loading factor does not strongly affect their results.

A fraction f_k of the feedback energy is added to the ejected mass as kinetic energy, while the rest is added as thermal energy. This naturally results in a jet velocity of

$$v_{\text{Jet}} = c \sqrt{2\epsilon f_{\text{kinetic}}} \quad (11)$$

or around $v \approx 0.045c$ for our fiducial parameter choices. Kinetic energy and the associated mass are put into the grid through two disks each of radius R_D located on either side of the AGN at a distance R_J from the center. The jets are oriented at a fixed angle ϕ_{Jet} with respect to the z axis and precess around it with a period τ_{jet} .

For simulations with pure thermal feedback ($f_k = 0$), we again follow the method of BS09 in order to prevent the injected thermal energy from immediately being radiated away. Feedback energy is stored up until enough accumulates to heat the gas in the injection zone to at least $T_{\text{min}} = 10^7$ K. Exploratory simulations with $T_{\text{min}} = 10^8$ did not show a noticeable difference in behavior, in agreement with BS09. We observe that this algorithm results in a series of thermal pulses as AGN feedback is ramping up, but comes close to steady injection when the AGN power is high. We performed tests using this injection threshold with some kinetic feedback ($f_k > 0.0$) but did not observe a noticeable difference when compared to simulations with continuous energy injection.

Unless otherwise noted we use the parameters given in Table 1 for all simulations.

2.4. Hydro Method

The simulations in this work use a 3D version of the ZEUS hydrodynamics method (Stone & Norman 1992) because of its robustness and speed. ZEUS is known to be a relatively diffusive method and requires an artificial viscosity term that may affect the accuracy of our hydrodynamics calculations. We have experimented with using a piecewise-parabolic method (PPM) (Colella & Woodward 1984), but encountered numerical difficulties relating to the strong discontinuities occurring at the injection site.

3. RESULTS

The most striking differences within our suite of simulations are between AGN feedback algorithms that deliver all of the feedback in thermal form ($f_k = 0$) and those that deliver at least some kinetic feedback ($f_k > 0$). Changes in the triggering method produce smaller differences in qualitative behavior, probably because all three triggering methods implemented here end up strongly boosting the feedback response when significant amounts of cold gas accumulate near the central black hole. We will therefore present our results on delivery mechanisms first and triggering mechanisms second.

3.1. Delivery of Feedback: Thermal vs. Kinetic

Injection of AGN feedback energy heats the surrounding gas through several processes. First, if $f_k < 1.0$, then the AGN directly injects thermal energy into the ICM. Second, interactions between the AGN outflow and the ICM produce shocks that propagate outward and heat the ambient gas in a quasi-isotropic manner. Third, outflows drive turbulence that can heat the ICM as the turbulence decays. Finally, momentum from the AGN outflow—either directly injected in the form of a kinetic jet or driven by thermal expansion of hot bubbles—can dredge low-entropy gas out of the core and mix it with higher entropy gas at larger radii.

3.1.1. Feedback Power

All of our simulations with $f_k > 0.0$ follow similar patterns of evolution. Initially, the cluster core is smooth, spherically symmetric, and contains no cold gas. The core gas then cools, contracts, and grows denser for ~ 0.3 Gyr until cold clouds begin to condense at the center and strongly boost the jet power. Figure 1 shows both the jet power and cooling luminosity within different radii during the first 2 Gyr of a cold-gas triggered feedback simulation that delivers 50% of the feedback power as kinetic energy. Notice that the core achieves approximate long-term balance when the jet power rises to match the cooling luminosity from within the central ~ 100 kpc. This is typical of our simulations that have a significant fraction of the feedback power in kinetic form. However, the total feedback power becomes much greater in simulations with purely thermal feedback.

Figure 2 illustrates the vast difference in feedback power between our simulations with $f_k = 0$ and those with $f_k > 0$. Pure thermal feedback eventually saturates at a power level more than two orders of magnitude greater than in the simulations with some kinetic feedback, even when compared to the case with $f_k = 0.25$. Furthermore, it can be seen that the average feedback power in the self-regulated systems with at least some kinetic power is not monotonically dependent on f_k . As long as some of the feedback power is kinetic, self-regulation happens at a power level of $\sim 10^{45}$ erg s $^{-1}$, which is similar to the time-averaged AGN power inferred from

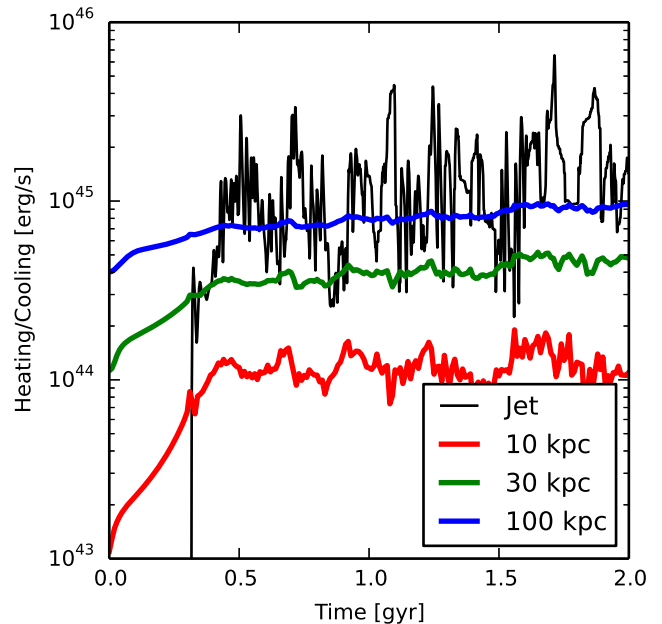


Figure 1. Total AGN power (thermal + kinetic) and cooling luminosity for a simulation with cold gas triggered feedback and $f_k = 0.5$. The jagged black line shows instantaneous jet power sampled every 5 Myr. Red, green, and blue lines show the total cooling luminosity of gas within 10, 30, and 100 kpc respectively, sampled at the same cadence.

observations of X-ray cavities in galaxy cluster cores (e.g., McNamara & Nulsen 2012).

3.1.2. Cold Gas Accumulation

Feedback power becomes excessively large in the $f_k = 0$ case because pure thermal feedback is ineffective at preventing large amounts of cold gas from accumulating. Figure 3 shows that $\sim 10^{12} M_\odot$ of cold gas accumulates in less than 1 Gyr when $f_k = 0$, whereas $\lesssim 10^{10} M_\odot$ accumulates during the same time period in simulations with at least some kinetic power. The large cold-gas reservoir in the $f_k = 0$ case is not sufficiently disrupted by thermal feedback and therefore provides enough cold fuel for the AGN to maintain a feedback power exceeding 10^{47} erg s $^{-1}$. Even at this power level, the AGN fails to eject or eliminate much of the cold gas because the cold gas is very efficient at radiating away feedback energy owing to the n^2 dependence of the cooling rate. The result is that the feedback energy that does go into the cold gas is almost immediately radiated away. Further, feedback energy tends to propagate more readily through the hot ambient medium along the paths of least resistance, and ends up increasing the thermal energy of the diffuse, volume-filling gas without diminishing the mass of cold gas embedded within it.

If star formation had been allowed to proceed in our simulations, much of the cold gas that accumulates near the center would eventually have formed stars. The results shown in Figure 3 therefore indicate that pure thermal feedback would permit a time-averaged star-formation rate $\sim 10^{2-3} M_\odot \text{ yr}^{-1}$ during the first ~ 1 Gyr, which is much larger than observed in all but the most actively star-forming galaxy cluster cores (O’Dea et al. 2008). In order to understand why kinetic feedback is so much more successful than thermal feedback in suppressing cold gas accumulation and the star formation that would result, we need to look at how the choice of f_k affects the radial distribution of density, temperature, and entropy in

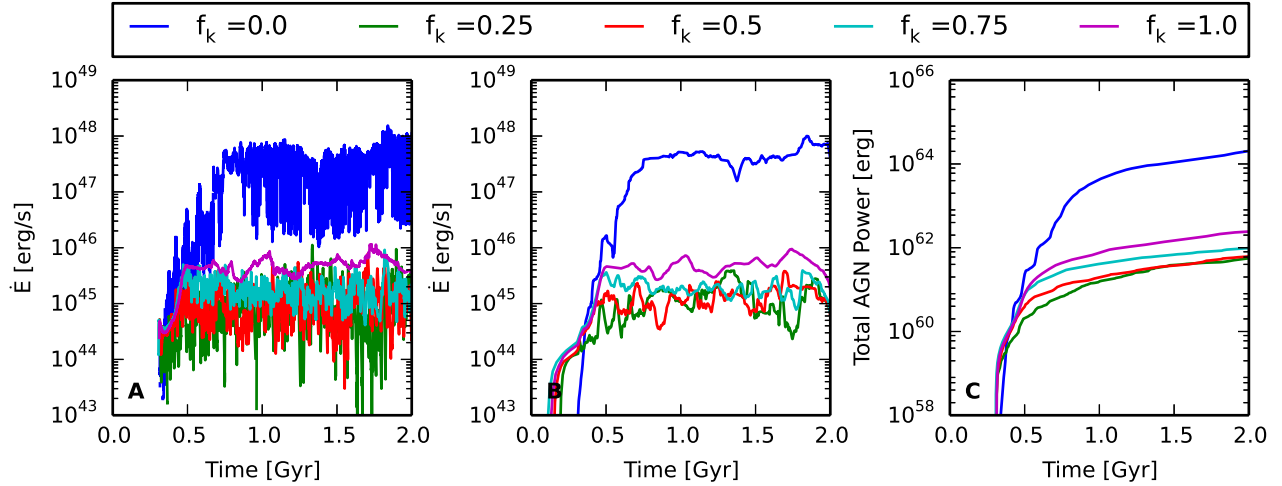


Figure 2. Feedback power (\dot{E}) (thermal + kinetic) as a function of time for simulations with cold gas triggering and varying values of f_k , the fraction of feedback power in kinetic form. Panel A shows the instantaneous value of \dot{E} . In Panel B, \dot{E} has been smoothed over a 50 Myr uniform smoothing kernel. Panel C shows the cumulative energy released by the AGN.

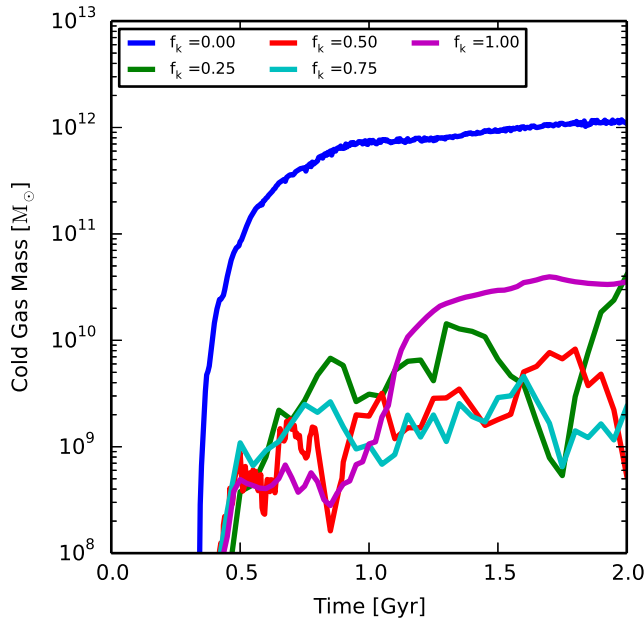


Figure 3. Total mass of cold gas as function of time for simulations with cold gas triggering and differing values of f_k . The amount of cold gas that accumulates in the simulation with $f_k = 0$ is two orders of magnitude greater than in any of the simulations with some of the feedback energy in kinetic form.

the hot ambient medium.

3.1.3. Radial Profiles

Figure 4 shows how the average values of density, temperature, entropy, and concentration of tracer fluid change over time at each radius in simulations with mixed kinetic and thermal feedback ($f_k = 0.5$, left panels) and pure thermal feedback ($f_k = 0$, right panels). Gas outside of ~ 100 kpc is not shown because it does not evolve appreciably over 2 Gyr, as the cooling time at large radii is long and little of the AGN feedback energy propagates to those radii. Inside of 100 kpc, the $f_k = 0.5$ simulation reaches a nearly steady state in ~ 0.5 Gyr, with density, temperature, and entropy continuing to fluctuate within narrow ranges after that time. The profiles of the tracer

fluid concentration do not reach a steady state, as the tracer is continuously injected over time and distributed outward by the jet. However, those profiles do show that tracer fluid is quickly mixed with the ambient gas out to $\gtrsim 50$ kpc from the center.

In contrast, the simulation with $f_k = 0$ does not reach a steady state. In particular, the azimuthally averaged specific entropy of gas outside of the central few kpc steadily rises with time, causing a steady drop in ambient density and a steady rise in ambient temperature. Initially, some of the increase in mean entropy comes from the removal of low-entropy gas through condensation (Voit & Bryan 2001; Voit et al. 2002; Nagai et al. 2007). However, the mean entropy at $\gtrsim 10$ kpc continues to rise during the second Gyr of the simulation, after condensation of cold gas has leveled off. This rise is due to continual input of thermal energy by AGN feedback, a small fraction of which escapes the inner few kpc and propagates into the ICM, causing pressure-driven expansion of the ambient medium. The right-hand panel of Figure 2 shows that AGN feedback in the $f_k = 0$ simulation has injected $\sim 10^{64}$ erg after 2 Gyr, which is comparable to the binding energy of the entire intracluster medium, although most of this is radiated away by the cold gas. The fraction that does escape the central clump of cold gas slows the condensation process by inflating the cluster core and driving the cooling time of the ambient medium at ~ 10 kpc to ~ 5 Gyr but fails to establish a self-regulated feedback loop.

Despite the high AGN power, this simulation is not able to prevent a buildup of cold gas for two reasons: (1) feedback energy does not propagate far enough from the center, and (2) thermal feedback cannot destroy a large cold-gas reservoir, once it develops. As illustrated in Figure 5, almost all of the cooling comes from the central 10 kpc where there is a concentration of cold gas with a very short cooling time. Although gas at the temperature floor does not cool, a small rise in temperature greatly increases its cooling rate and prevents the cold gas from heating to the ambient temperature.

The development of a large cold-gas reservoir is closely related to the failure of thermal feedback to propagate feedback energy beyond the central ~ 30 kpc. Figure 6 shows the rms gas velocity as a function of radius in simulations with dif-

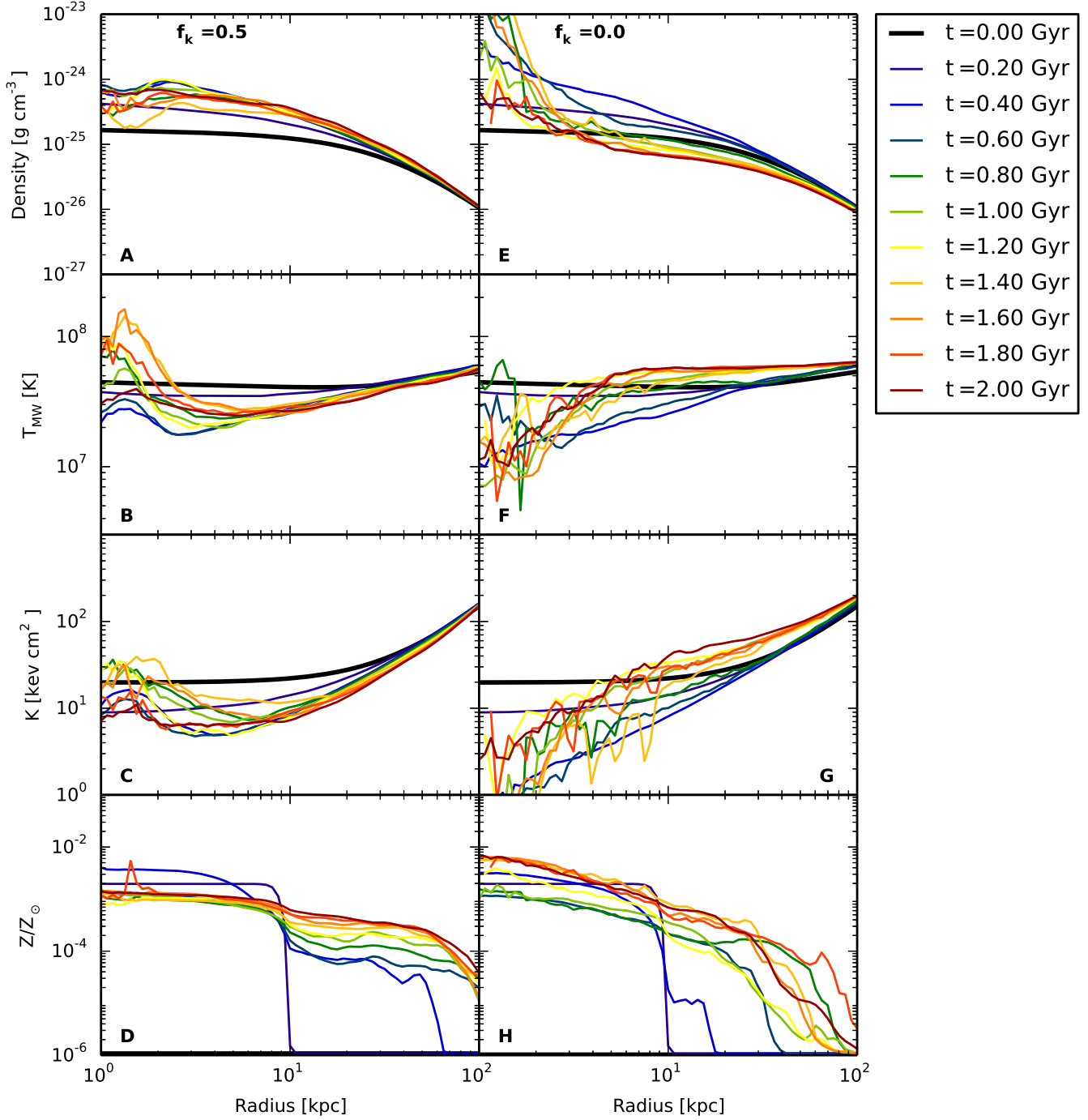


Figure 4. Profiles of various quantities as the simulation evolves for simulations with $f_k = 0.5$ (left) and $f_k = 0.0$ (right) with cold gas triggering. Thick black lines denote the initial conditions, while other line colors indicate values at later times. Density is weighted by volume, temperature by mass, and metallicity by mass. Entropy is computed using the volume weighted temperature and the mass weighted density, as discussed in Section 3.2.3 of Skory et al. (2013).

ferent proportions of kinetic feedback ($f_k = 0.0, 0.5,$ and $1.0,$ respectively). In the pure thermal case, there is a sharp drop in rms velocity beyond ~ 30 kpc which is not seen in the simulations having some kinetic feedback. Apparently, kinetic feedback is more effective at transporting feedback energy to large radii.

This discrepancy arises because outward propagation of centrally injected thermal feedback is limited by the amount of entropy it can generate. It creates central bubbles of hot gas which can buoyantly rise only until they reach a layer of

equivalent entropy. Then the bubbles blend with their surroundings. In this set of simulations, centrally injected hot bubbles stop rising and blend with the ambient medium at ~ 30 kpc, as indicated by the rms velocity curves in Figure 6, as well as the propagation of tracer fluid in panel H of Figure 4. We therefore conclude that our implementation of pure thermal feedback does not add much heat to gas in the 30–100 kpc range of radii but instead steadily raises the entropy of ambient gas at 10–30 kpc, which flattens its entropy gradient. Kinetic feedback, on the other hand does propagate beyond

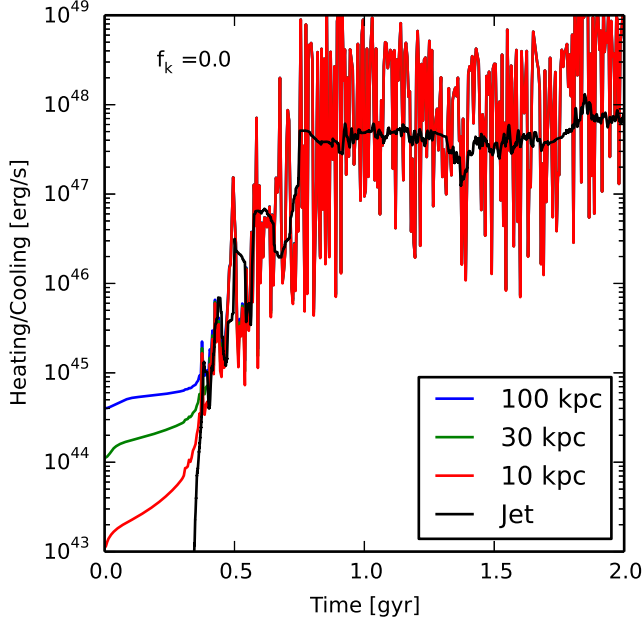


Figure 5. The radiative cooling rate of the gas within different radii is compared to the total jet power (thermal + kinetic) for the simulation with $f_k = 0.0$. At times greater than 0.5 Gyr, all of the cooling is occurring within 10 kpc, and the three lines overlap.

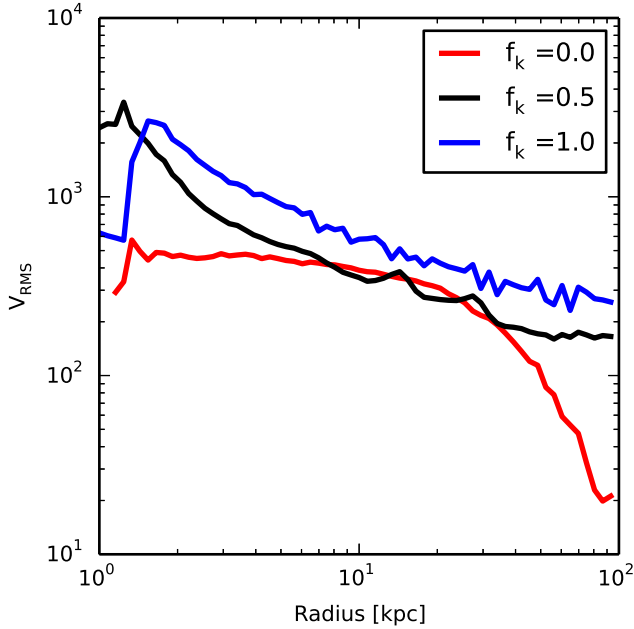


Figure 6. Mass weighted profile of RMS velocity in the hot ambient medium for simulations with cold gas triggering and different kinetic fractions. All profiles are computed 1.75 Gyr after the beginning of the simulation.

30 kpc and consequently allows gas in the entire 10–100 kpc range to settle into a quasi-steady, self-regulated state.

3.1.4. Jet Precession

In addition to the breakdown between kinetic and thermal feedback, we have also investigated the role of jet precession. Jets from AGN can reorient themselves on timescales of a few tens of Myr (Dunn et al. 2006; Babul et al. 2013), but the details of this process are still uncertain, and our subgrid model

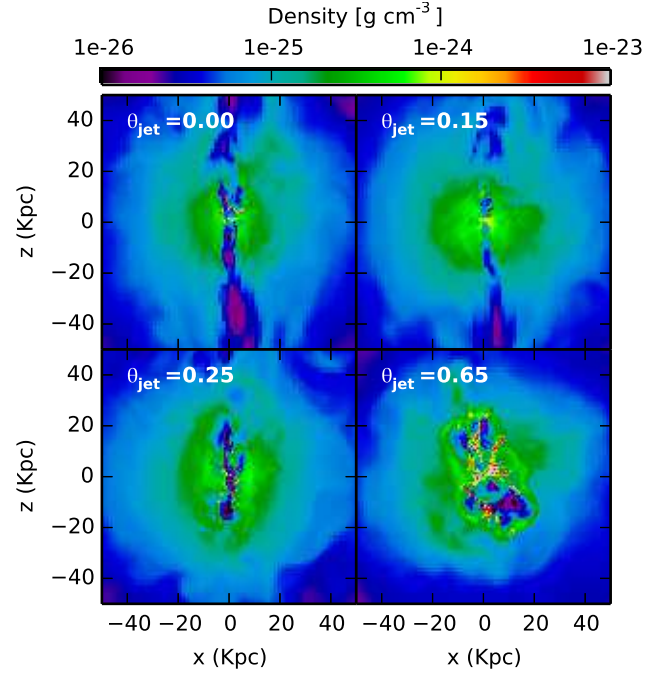


Figure 7. Density slices for simulations with different values of θ_{jet} . In our model, the AGN jet precesses around the z axis with a period of 10 Myr at a constant angle θ_{jet} with the z axis. All simulations use cold gas triggering and have $f_k = 0.5$.

and idealized setup are not capable of self-consistently modeling jet precession. Instead, we follow Li & Bryan (2014a) and force the jets to precess around a fixed axis. Previous studies have found that some precession is necessary for self-regulation if the jets are highly collimated. Otherwise, they drill long, narrow channels through the ICM and deposit the bulk of their energy far from the zone in which self-regulation can happen Vernaleo & Reynolds (2006).

Figure 7 shows slices of four simulations performed with different jet precession angles. When the jets do not precess ($\theta_{jet} = 0$), they carve channels through the ICM that extend well beyond ~ 40 kpc. However, due to Kelvin-Helmholtz instabilities and artificial viscosity in the ZEUS code, they still produce some heating close to the AGN but do not drive strong shocks. With a small precession angle ($\theta_{jet} = 0.15, 0.25$), each jet continually encounters cold clouds of condensing material that block its path. These jet-cloud interactions randomly divert the jets, depositing their energy in a wider range of directions, which causes more of their kinetic energy to thermalize at smaller radii. Precession also produces more turbulence and creates shocks that propagate outward over a large range of solid angles. As the precession angle increases, the jet energy spreads over a larger range of solid angles at ever smaller radii, and jet-cloud collisions become more frequent. As seen in the last panel of Figure 7, this leads to a more disturbed morphology at $\lesssim 20$ kpc and a larger mass of accumulated cold gas. In that respect, kinetic feedback with a very large precession angle becomes more like thermal feedback, in that feedback energy does not propagate as far from the center before it becomes thermalized.

3.2. AGN Triggering Mechanisms

We do not see strong differences between our simulations with different AGN triggering mechanisms, as long as we are using a maximum spatial resolution of 196 pc (see Figure 8). This is likely a consequence of being able to resolve the mul-

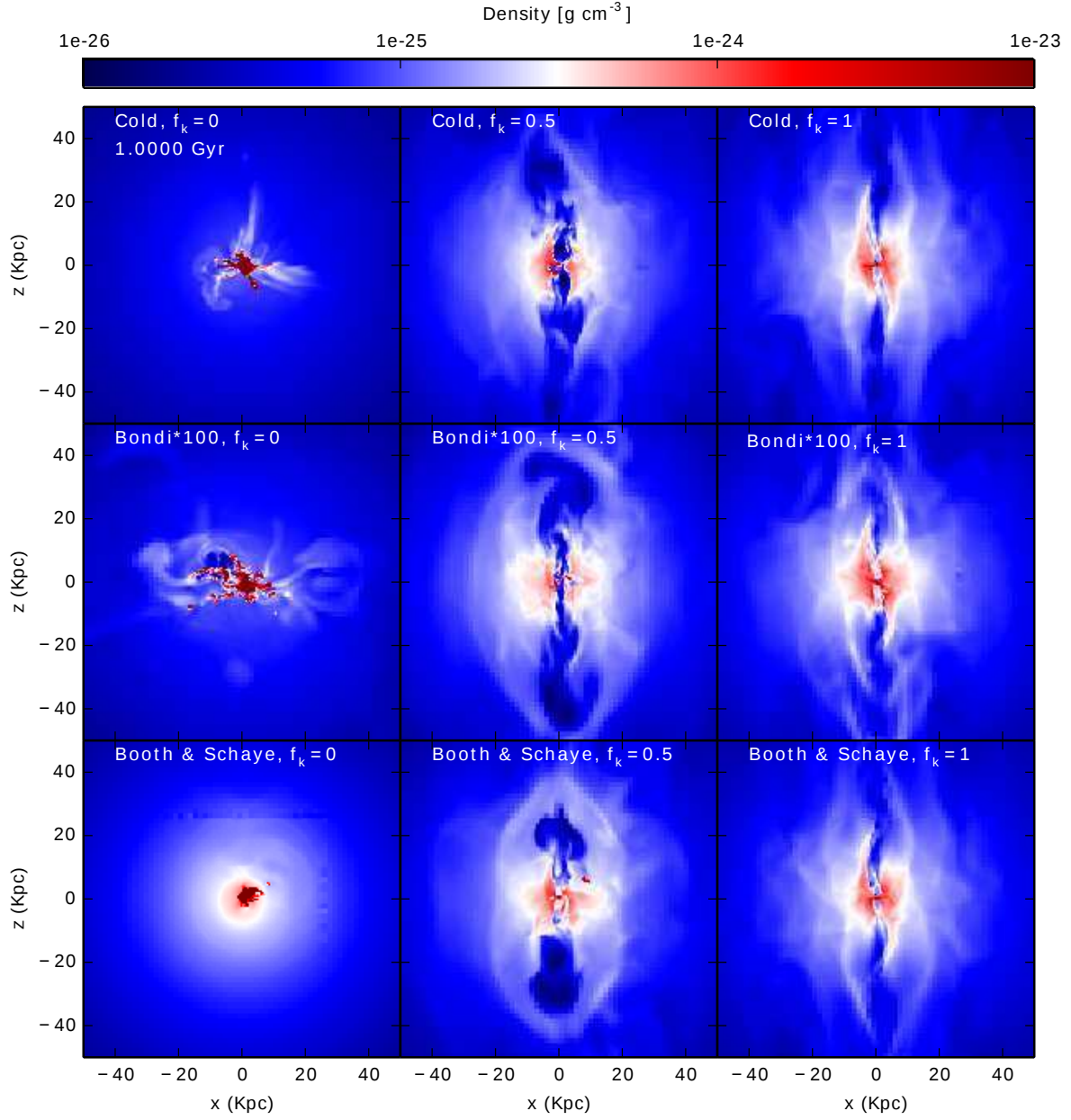


Figure 8. Slices of density through 9 simulations with different triggering mechanisms and kinetic feedback levels. All simulations are shown 1 Gyr after the beginning of the run. Simulations in the top row are triggered by cold gas accretion, the middle row by Bondi accretion with a constant boost factor, and the bottom row using the method of BS09. f_k gives the fraction of the feedback that is returned as kinetic energy.

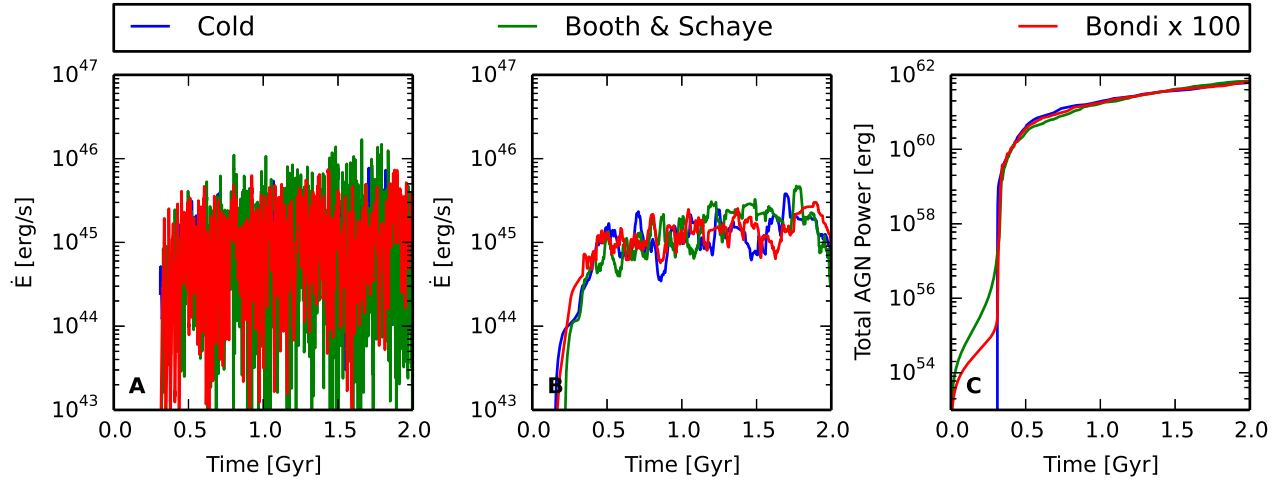


Figure 9. Like Figure 2, but for simulations with different triggering mechanisms. All simulations have $f_k = 0.5$. As in Figure 2, Panel A shows the instantaneous value of \dot{E} , Panel B shows \dot{E} smoothed over 50 Myr, and Panel C shows the cumulative jet power.

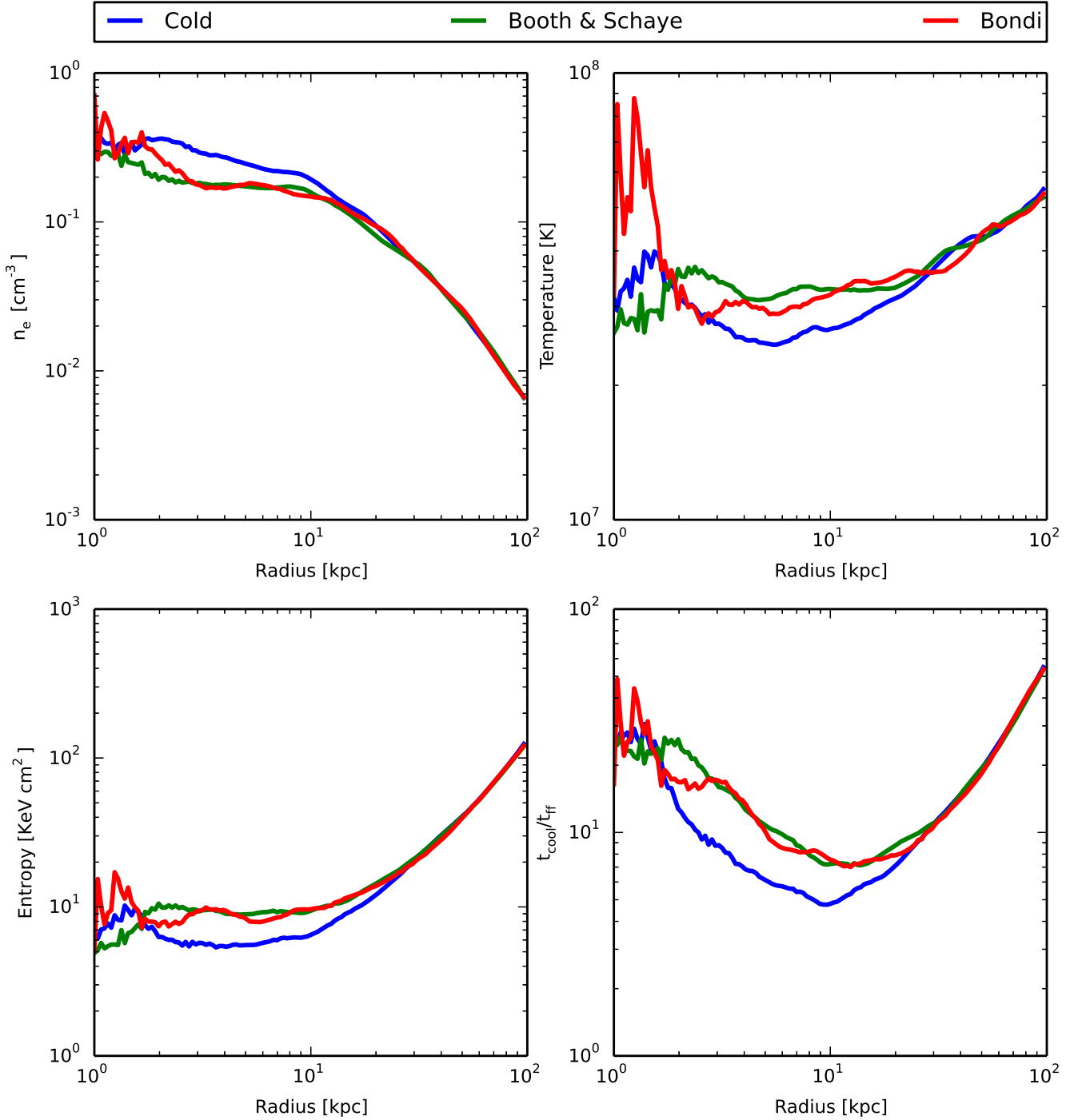


Figure 10. Profiles of different quantities for simulations with different triggering mechanisms after 2 Gyr. All simulations use $f_k = 0.5$. n_e is weighted by volume, while the other profiles are weighted by mass. All profiles excise gas below 3×10^4 K.

tipphase medium in the region surrounding the AGN. Since all of the triggering mechanisms considered are dependent on gas density, a cold, dense clump of gas accreting will trigger a large outburst regardless of the details of the triggering algorithm. The outburst will continue until the cold gas is gone, ensuring that roughly the same amount of energy is released in all cases. The cold gas would not necessarily be resolved by simulations with coarser resolution, implying that those simulations might be more sensitive to the choice of triggering algorithm.

Each triggering mechanism depends on gas density either directly (BS and Boosted Bondi-like accretion) or indirectly (cold gas triggering), and in the BS and Boosted Bondi-like cases the boost parameters have been chosen to provide the “right” amount of feedback. Due to the density-dependent accretion rate, a cold clump falling into the accretion zone then always produces a surge in jet power that continues until the clump is either completely heated or completely accreted.

Figure 9 shows total jet power (thermal + kinetic) versus time for simulations with different triggering mechanisms. In

the Bondi-like and BS runs, feedback is always active, but the power level is relatively low before cold gas starts to condense and drives up the AGN accretion rate. After condensation begins, all three triggering mechanisms lead to self-regulated jet power levels that are nearly identical. Figure 10 shows the radial profiles of various quantities in the ambient hot ICM after 2 Gyr for each triggering mechanism. There are some differences in the inner 10 kpc, but this zone is strongly affected by the quickly varying jet, producing profiles that are variable with time (see Figure 4). Between 10 and 30 kpc, the run with cold-gas triggering is slightly colder and more susceptible to thermal instability than the other runs, based on the lower $t_{\text{cool}}/t_{\text{ff}}$ ratio. Beyond 30 kpc, there are no significant differences between runs with different triggering mechanisms.

3.3. Accretion Radius

In cosmological simulations of galaxy cluster evolution, one would like a subgrid model for AGN feedback that gives reliable results for the SMBH accretion rate even when the Bondi radius (let alone the Schwarzschild radius) is not resolved. At spatial resolutions coarser than ~ 0.5 kpc, the size of the “accretion zone” that determines AGN feedback power will necessarily be larger than that used in our fiducial simulations. With this increase in R_{acc} , the responses of AGN triggering algorithms will depend on conditions at larger radii, which can couple AGN feedback to ICM properties at greater distances but may also permit larger amounts of gas to condense before the AGN feedback response becomes strong enough to oppose cooling.

To understand how the size of the accretion zone affects AGN triggering, we have carried out simulations in which R_{acc} is increased to 2 kpc. The maximum spatial resolution remains the same, with a smallest cell width of 196 pc, meaning that the accretion radius is always resolved by multiple cells. In carrying out these simulations we set the distance R_j of the disk-shaped jet injection region equal to R_{acc} , so that the jet emanates from the edge of the accretion sphere, not from within it.

Figure 11 shows jet power as a function of time for the simulations with a larger accretion radius. In all three simulations, fluctuations in jet power are noticeably smaller than in the fiducial case. With the exception of the Boosted Bondi-like run the cumulative jet power is comparable to the earlier runs, and we did not observe quantitative differences in the ICM properties. However, the Boosted Bondi-like simulation, in which AGN feedback power now depends on average gas properties within a larger volume, takes longer to ramp up, resulting in a large ($> 10^{12}$) mass of cold gas and a higher cumulative jet power.

4. DISCUSSION

Our simulations have shown that different triggering and delivery methods for subgrid models of AGN feedback can have profoundly different effects on the resulting properties of the ICM. We are not attempting to determine which method is the most accurate model of an AGN but rather to analyze the reasons for those differences. In each case, tracking the accumulation of cold-gas fuel is critical, meaning that we must consider what allows gas to transition from the hot ambient medium into the cold-gas fuel reservoir. In this section, we discuss that transition and consider the potential effects of physical processes not included in our models.

4.1. Precipitation and AGN Fueling

Clearly, our simulations with pure thermal feedback behave markedly differently than simulations with kinetic feedback, even when f_k is small. The pure thermal feedback runs experience a large buildup of cold gas that essentially smothers the AGN, causing it to fight back with increasingly powerful bursts. The ICM in the vicinity of the AGN is subject to both radiative cooling and heating from mixing, dissipation, and shocks. Thus, analyzing the thermal stability of the ICM may give insight into the accumulation of cold gas and help to explain the differences that arise from among these feedback algorithms.

Voit et al. (2015) presented evidence for a “precipitation triggered” model for coupling the AGN power to the cooling rate of the ICM. In the precipitation model, the cooling ICM becomes thermally unstable, leading to the condensation of cold gas. This cold gas is then accreted by the AGN, triggering feedback. The feedback heats the ICM, restoring thermal stability and reducing further accretion. As cosmological simulations typically lack the resolution to model the condensation process itself, the thermal instability criterion can be used to predict the amount of cold gas available for accretion. For a gravitationally stratified medium, one would expect that thermal stability would be related to two natural timescales — the cooling timescale t_{cool} and the dynamical timescale t_{ff} . Simulations (McCourt et al. 2012; Sharma et al. 2012) find that the formation of cold gas from a thermally unstable medium can occur whenever $t_{\text{cool}}/t_{\text{ff}} \lesssim 10$ (But see Meece et al. (2015), which finds that condensation can occur for larger values in some circumstances.) Similarly, the observations of Voit & Donahue (2015) and Cavagnolo et al. (2008) show that clusters with $t_{\text{cool}}/t_{\text{ff}} \lesssim 10$ are likely to exhibit multiphase gas, while clusters above that ratio do not.

Figure 12 shows the distributions of $t_{\text{cool}}/t_{\text{ff}}$ and specific entropy (K) for simulations with pure thermal ($f_k = 0.0$) and part kinetic ($f_k = 0.5$) feedback. Panel A of Figure 12 shows that the ICM in the thermal feedback simulation is divided into two phases. First, there is a hot phase with $t_{\text{cool}}/t_{\text{ff}} \gg 10$ that occupies the bulk of the volume outside of 10 kpc. Second, there is a large accumulation of cold gas that nearly smothers the AGN. The cold gas mass builds up quickly and then stops growing when the cooling time in the hot ICM rises to several Gyr. Outbursts of thermal feedback sporadically propel streamers and blobs of cool gas radially outwards from the AGN. These cold streamers travel out several tens of kpc before turning around and raining back down onto the core. Panel C shows that there is a large spread in $t_{\text{cool}}/t_{\text{ff}}$ and K in the 10–30 kpc range. Most of the gas at intermediate values of $t_{\text{cool}}/t_{\text{ff}}$ does not represent condensation in the usual sense. Instead, it is gas in the boundary layers of the streamers that is either cooling onto them or being heated by interactions with the hot ICM.

As Panels B, D, and F of Figure 12 illustrate, the gas properties of the ICM for the simulation with $f_k = 0.5$ are very different. The ICM has much lower mean values of $t_{\text{cool}}/t_{\text{ff}}$ and K at each radius out to 30 kpc. Panel B is typical of the state of the cluster after the jet has formed, with the volume in which $t_{\text{cool}}/t_{\text{ff}} \lesssim 10$ occupying a roughly spherical region of radius ~ 20 kpc, excluding a hot channel near the jet axis. Overall radiative losses are nearly balanced by gentle shock heating over several cooling times. However, at radii of ~ 10 kpc, where $t_{\text{cool}}/t_{\text{ff}}$ reaches a minimum value $\lesssim 10$, we observe relatively small amounts of condensing gas. Consis-

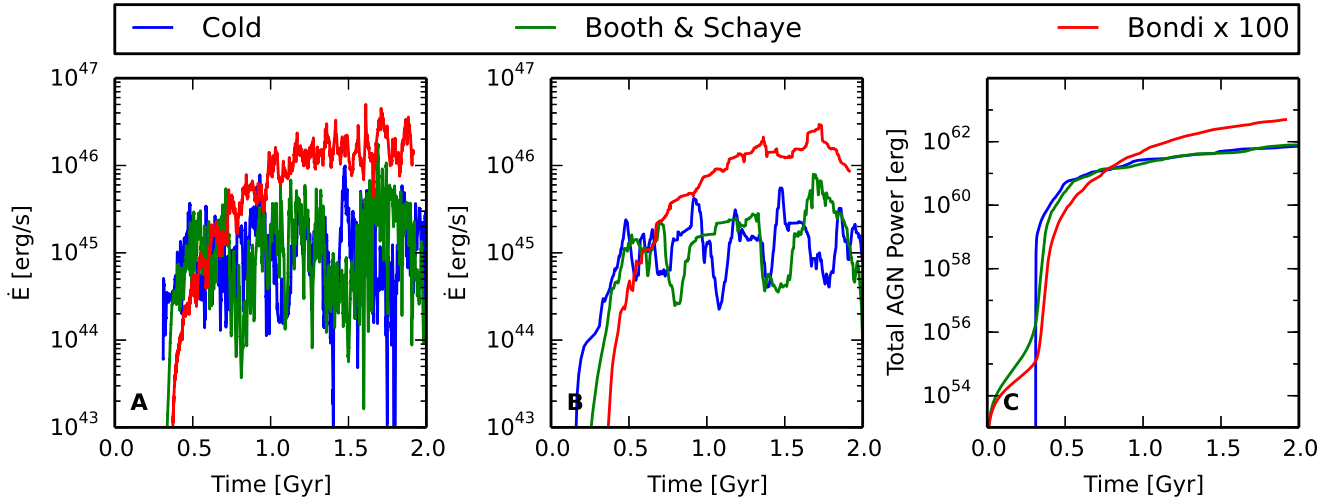


Figure 11. Jet power vs. time for simulations with $r_{acc} = r_{disk} = 2$ kpc. All simulations have $f_k = 0.5$. Like in Figure 2, Panel A shows the instantaneous value of \dot{E} , Panel B shows \dot{E} smoothed over 50 Myr, and Panel C shows the cumulative jet power.

tent with Li & Bryan (2014b), this condensation occurs at the jet/ICM interface where the jet generates non-linear entropy fluctuations by uplifting low-entropy gas close to the AGN to greater heights, where it then condenses and falls back toward the center. These condensates are then accreted by the AGN, powering the jets and maintaining thermal balance in the cluster.

The dramatic differences in the behavior of the cold gas and the jet in these simulations has to do with how the AGN distributes energy to the surrounding gas. In the pure thermal feedback case, the gas heated by the AGN at first tends to follow the path of least resistance, bypassing the denser gas near the core. This leads to an accumulation of cold gas with a very short cooling time, which is able to absorb and reradiate the AGN feedback at later times. The AGN injects energy very close to the center of the cluster, where it is immediately radiated away by cold gas. In the (f_k) simulation, the outflow creates a hot cocoon around itself that rapidly rises. This outflow lifts the central gas outward, which helps disrupt the cooling flow and pulls some low-entropy gas upward along with the jets. The kinetic outflow also allows the feedback energy to penetrate to larger radii (> 10 kpc) and heat the ICM at greater radii. This helps to maintain the balance of heating and cooling globally and prevents the ICM from dividing into a hot and a cold phase. The jet is able to heat gas further out, through mixing, turbulent decay and weak shocks, which prevents the cooling time of a large fraction of the ICM from going below $10t_{ff}$. Thus, a cluster with a warmer, less dense core will require less energy input to regulate than a cluster with a cold, dense core.

In addition to depositing feedback further out, the kinetic outflows allow cooling gas to mix with the hot gas in the jet. This increases the cooling time of the ICM and strongly inhibits the formation of more cold gas. The cold or cooling gas that is not accreted is soon swept up in the jet, where it is disrupted or heated. The jet thus prevents the cold gas from smothering the AGN, allowing the feedback to heat the ICM rather than quickly radiating away. This explains why a weaker AGN is able to regulate the ICM in the kinetic jet case than in the more powerful pure thermal feedback case.

4.2. Caveats and Additional Physics

In this study, both our setup and our implementation of AGN feedback have been simplified in order to focus on the essential features of coupling between the AGN and the ICM. Of course, the situation in real clusters is more complicated than our model. In addition to these simplifications, there are a number of possibly relevant physical processes that we have not included in our model, both to simplify the problem and to reduce the computational resources required. These processes and their potential effects are discussed in this section.

4.2.1. Conduction

Our simulations do not include thermal conduction, either isotropic or along magnetic fields. From a theoretical point of view (Voit et al. 2015, 2008), while conduction may well be important for regulating the thermal state of warm-core clusters, cool-core clusters lie below the t_{cool} profile at which conductive transport can balance radiative losses. Smith et al. (2013) has simulated cool-core clusters with thermal conduction but without AGN feedback, and concludes that thermal conduction is not able to prevent the cooling catastrophe on its own and does not have a large impact on global cluster properties. However, conduction could well be important for the precipitation theory, as strong conduction could smooth out the perturbations that evolve into non-linear overdensities. Wagh et al. (2014) have investigated the effects of conduction on thermal stability and found that conduction would need to be quite strong to prevent condensation.

4.2.2. Magnetic Fields

The intra-cluster medium is known to be weakly magnetized (Carilli & Taylor 2002). Overall, the magnetic field is believed to be tangled and dynamically unimportant. However, magnetic fields may affect heat transport in the core by making conduction anisotropic, as the electrons that mediate conduction will travel more easily along field lines than perpendicular to them. The importance of anisotropic conduction will depend on the magnetic field configuration, the development of plasma instabilities, and stirring of the plasma by galaxy motions or AGN outflows. A tangled magnetic field would be expected to suppress conduction to roughly 1/3 of the Spitzer value. However, a weakly magnetized, conducting ICM with a temperature gradient might be susceptible

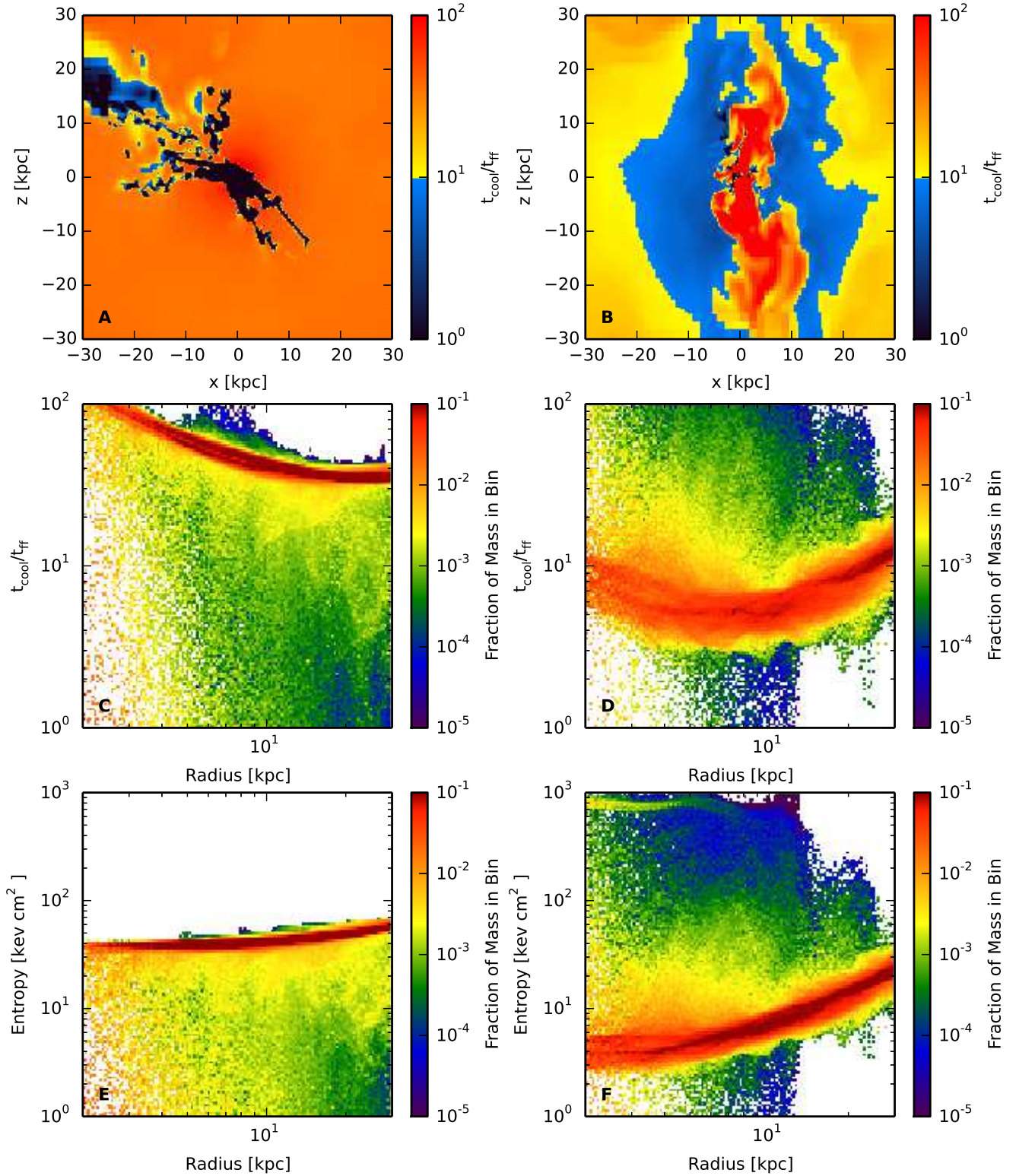


Figure 12. Distribution of the $t_{\text{cool}}/t_{\text{ff}}$ ratio for simulations with cold triggering and either $f_k = 0.0$ (left column) or $f_k = 0.5$ (right column), shown at 1.46 Gyr after the beginning of the simulation. Panels A and B show slices of the local $t_{\text{cool}}/t_{\text{ff}}$ for each simulation. The color-break in the scale at $t_{\text{cool}}/t_{\text{ff}} = 10$ indicates the precipitation threshold identified by earlier studies. Panels C and D show the distribution of $t_{\text{cool}}/t_{\text{ff}}$ values normalized by the total mass at each radius. The colors show the mass in each bin divided by the total mass in that radial shell. Similarly, Panels E and F show the Entropy distribution. Cold gas ($< 3 \times 10^4$ K) is excluded from the analysis.

to either the magnetothermal instability (MTI; Balbus 2000, 2001; Quataert 2008) or the heat-flux-driven buoyancy instability (HBI; Quataert 2008; Parrish et al. 2009). In cool-core clusters, the HBI would align the magnetic field perpendicular to an outward temperature gradient, limiting the inward heat flux. However, simulations such as Ruszkowski et al. (2011) have found that anisotropic thermal conduction is not strong enough to reorient the magnetic fields, and Yang & Reynolds (2015) find that stirring by the AGN would overcome the HBI, leading to conduction with an effectiveness of > 0.2 times the Spitzer value.

While not dynamically important on large scales, magnetic fields may affect the precipitation and AGN feedback processes. Wagh et al. (2014) found that anisotropic conduction will not prevent condensation unless the field is very strong. Magnetic fields may be stronger and dynamically important close to the AGN, where jet induced turbulence and field injection from the jet may amplify the magnetic field (Dubois et al. 2009; Sutter et al. 2012; Ruszkowski et al. 2011). Along the AGN jets, magnetic draping is thought to play an important role in preserving cavities and cold fronts against disruption from Kelvin-Helmholtz instabilities (Ruszkowski et al. 2007; Dursi & Frommer 2008). The preservation of cavities would change the mode of heat transport in the cluster, because inflating cavities and rising bubbles would be better able to stir turbulence, transport hot gas to larger radii, and dredge up cold gas in their wake.

4.2.3. Star Formation

BCGs in many cool core clusters are observed to be forming stars (O’Dea et al. 2008, 2010; Loubser et al. 2015; McDonald et al. 2015), but stellar feedback alone can not prevent the cooling catastrophe in cool-core clusters (e.g. Skory et al. 2013). Although we do not include star formation in our model, Li et al. (2015) use a setup very similar to our fiducial model to perform an extensive investigation of the role of star formation in regulating AGN feedback. One expects the star formation rate (SFR) of a BCG to be related to the amount of multiphase gas present. Li et al. (2015) do see a correlation between AGN feedback and the SFR. In those simulations, stellar feedback is less effective than the AGN at heating the ICM but more effective at consuming cold gas. If the AGN is in a low-power state, a central reservoir of cold gas builds up and boosts the AGN power on a ~ 100 Myr timescale. AGN feedback then heats the ICM and slows the rate of gas condensation. However, the AGN remains powerful until star formation consumes the cold gas in the central reservoir on a ~ 2 Gyr timescale. Without cold clouds to fuel it, the AGN feedback power subsides, and another cycle soon begins as the ambient medium once again cools and becomes thermally unstable. Thus, the primary effect of star formation is to regulate the cycling behavior of the AGN on Gyr timescales.

4.3. Comparison With Similar Studies

As the importance of AGN feedback has gained greater appreciation in recent years, several studies have been carried out to investigate the best way to implement AGN feedback in simulations. It is difficult to do a comprehensive comparison between our results and those of previous studies as those works have generally sampled a limited fraction of the AGN feedback parameter space or assume vastly different initial conditions than we do here.

The chief aim of this paper is to better understand which aspects of AGN feedback implementations are most decisive in determining the qualitative consequences of sub-grid models for AGN feedback. With this in mind, we discuss the major differences between our implementation and some AGN implementations used in related studies of AGN feedback. Where possible, we compare our results to those obtained using these other algorithms. Note that in addition to the major differences discussed here, there are many other small differences in the details of how AGN feedback is implemented and in the choices of physical models considered. As demonstrated by Section 3, the results of an AGN feedback simulation may be sensitive to seemingly small differences in implementation, and caution should be taken when comparing one set of results to another.

4.3.1. Li & Bryan 2012-2015

The cluster and AGN model employed in our paper are largely an extension of the Li & Bryan simulations of AGN feedback (Li & Bryan 2012, 2014a,b; Li et al. 2015), with only small changes to the cluster and jet model (although we extend the range of triggering and feedback parameters). Both our study and theirs use Enzo.

Given the similarities of our setups, it is not surprising that our simulations give similar results. Our maximum spatial resolution is slightly coarser (196 pc vs. 60 pc), but we obtain similar behavior for similar choices of feedback parameters. Our findings indicate that the Li & Bryan results should be relatively insensitive to variations in the triggering mechanism, the amount of AGN precession, and the details of the accretion process. Both studies find that the behavior of the AGN is relatively insensitive to the kinetic fraction of the outflow as long as the kinetic fraction is non-zero. Our study does find that the mass of cold gas formed depends strongly on the AGN implementation, but does not affect the long term behavior of the simulation. We generally see a mass of cold gas that is an order of magnitude less than what Li & Bryan found in their fiducial model but obtain a similar mass when we use the same set of parameters. This variability in the cold gas mass is consistent with the parameter variation studies in Li & Bryan (2014a).

4.3.2. Gaspari et al. 2011

Gaspari et al. (2011b) simulate AGN feedback using the FLASH code (Fryxell et al. 2000). They model an idealized version of the cluster Abell 1795 within a static and spherically symmetric gravitational potential using a set of physical processes similar to those used here. The minimum resolution in their study is 2.7 kpc. AGN feedback is modeled as a purely mechanical jet with either cold or hot (Bondi-like) triggering and different jet efficiencies. They also consider both steady and intermittent jets. For Bondi-like triggering, the accretion rate is calculated from the properties of gas within 5 or 10 kpc. Gaspari et al. (2011a) uses a similar AGN model but a gravitational potential appropriate for a galaxy group.

Gaspari et al. (2011b) finds that both a cold gas triggered and a Bondi triggered AGN implementation are able to balance radiative cooling and preserve a cool-core state. The most successful cold gas model (model A3 in that paper) is significantly more bursty than our simulations, with a duty cycle of only 6%, resulting in only around 50 outbursts each with power on the order of 10^{48} erg/s. The total injected energy after 2 Gyr is on the order of 10^{61} erg, consistent with

our results. We attribute the observed difference in outburst power and duty cycle to the choice of accretion radius, where we use 0.5 kpc and they use 10 kpc. As seen in Figure 11 in our paper, increasing the size of the accretion radius results in a larger variation in AGN power. This follows from more cold gas being able to fit inside the larger accretion zone and from the difficulty of expelling cold gas from a larger gravitational well.

In agreement with our results, Gaspari et al. (2011b) finds that Bondi feedback with a large averaging zone (10 kpc in their simulations) is not able to halt the cooling catastrophe. Their model with an averaging zone of 5 kpc is able to balance cooling over a long period of time. Unlike the cold gas triggered case, the Bondi implementation results in a low power (order 10^{44} erg/s) jet with little variation in intensity. In our simulations, the Bondi and cold-triggered implementations act similarly when using an accretion radius/averaging zone of 0.5 kpc. We ascribe this to the higher resolution of our simulations, which are able to resolve the cold gas directly.

4.3.3. Yang et al. 2012

Yang et al. (2012) examines the effect of different AGN subgrid models on observable properties of simulated galaxy clusters. They model an idealized cluster with virial mass $1.5 \times 10^{14} M_{\odot}$ and a polytropic equation of state, also using FLASH. The minimum resolution of these simulations is 1.0 kpc. The physical processes considered are again similar to ours, while the AGN feedback model is somewhat different, consisting of either large (tens of kpc) thermal bubbles offset from the core or jets with widths of a few kpc. The accretion rate was determined from the Bondi rate, with a constant boost factor ranging from 1 to 100 in different runs.

Although Yang et al. (2012) do consider jets with pure thermal feedback (as well as thermal bubbles originating near the AGN), they do not see the same smothering behavior that we do. In fact, the gas in their simulations does not become very dense, rarely exceeding densities of $n_e = 10^{-1} \text{ cm}^{-3}$. We attribute these differences to the finer resolution of our simulations, which allow us to resolve the condensation process and the formation of cold gas near the AGN.

4.3.4. Dubois et al. 2012

Dubois et al. (2012) compare thermal and mechanical feedback in cosmological simulations using the code RAMSES. The simulations generally have a minimum resolution of 1.52 kpc, but some runs have higher resolution. The AGN power is determined using the BS09 method. Thermal energy is released in a sphere of a few cells near the AGN, while kinetic feedback is released in a jet. Similar to Yang et al. (2012), they do not observe AGN smothering, but again employ a coarser resolution than we use in our simulations.

5. CONCLUSIONS

We have carried out a controlled comparison of several commonly used sub-grid implementations of AGN feedback. Our model treats the AGN as a particle sitting in the core of an idealized cool-core cluster. The AGN is triggered based on local conditions (either the amount of cold gas or the Bondi rate, with either a fixed or a density dependent boost) and returns energy to the ICM as either centralized thermal blasts, a kinetic jet, or a mix of thermal and kinetic energy. Our main conclusions are:

1. Purely thermal feedback produces very different results than feedback with even a small kinetic component. In the pure thermal case, the AGN is initially unable to inhibit cooling immediately outside of the core, leading to a buildup of cold gas. This gas smothers the AGN and immediately radiates away the feedback energy, even if the feedback zone itself is heated to a high temperature. This also results in heating of the ICM outside of the core through a combination of shock heating and preferential condensation of low entropy gas. Adding a kinetic component allows the AGN to propagate energy outside of the core and prevents smothering of the AGN.
2. When some fraction of the feedback is returned as a kinetic jet, the AGN is able to prevent the large accumulation of cold gas that results from a cooling catastrophe. Instead, AGN feedback self-regulates the ICM in a quasi-steady state with $t_{\text{cool}}/t_{\text{ff}} \sim 10$ at $\lesssim 20$ kpc. The cluster core is cooler overall than the case with pure thermal feedback, but contains much less cold gas around the AGN.
3. We do observe large differences between cold-gas triggered feedback, boosted Bondi-like triggering or Booth and Schaye accretion, as long as the ‘‘accretion zone’’ used to determine the AGN fueling rate is sufficiently small (~ 200 pc). This is probably because all three methods, by design, end up triggering strong AGN feedback when cold clouds begin to accumulate in the accretion zone.
4. Increasing the size of the accretion zone (to 2 kpc) reduces short-term variation in jet power but does not significantly alter the total amount of AGN feedback or the global ICM properties in the cold-gas triggered or Booth and Schaye cases. However, the boosted Bondi-like simulation does not achieve self-regulation, because AGN feedback does not ramp up fast enough to prevent a cooling catastrophe, resulting in a large central accumulation of cold gas.
5. Very large jet precession angles distribute the AGN feedback energy, making simulations with significant kinetic output behave more like simulations having pure thermal feedback. This happens because the kinetic energy does not escape to large radii and thermalizes closer to the AGN when it is spread over too large a solid angle.

Further improvements to sub-grid feedback models and a better understanding of the AGN feedback process are necessary for the next generation of galaxy and galaxy cluster simulations. On a theoretical level, much work is currently being done on the link between thermal instability, cold gas formation, and its role in triggering feedback. Ongoing observations with Chandra and XMM-Newton as well as future observations with the Smart-X and Athena missions will give a better understanding how the AGN feedback process operates in real clusters. Finally, new implementations must be developed for capturing the connection between AGN and their environments. While the simulations in this work have a maximum resolution of ~ 200 pc, cosmological simulations and simulations with more complicated physics generally have \gtrsim kpc resolution due to computational resource limits. In

future work, we will aim at translating the results from this project into a sub-grid implementation that can be used at these coarser resolutions.

6. ACKNOWLEDGMENTS

The authors would like to thank Gus Evrard, Mateusz Ruzskowski, Greg Bryan, and Yuan Li for helpful discussions during the preparation of this paper. This work was supported in part by Michigan State University through computational resources provided by the Institute for Cyber-Enabled Research. BWO was supported in part by the sabbatical visitor program at the Michigan Institute for Research in Astrophysics (MIRA) at the University of Michigan in Ann Arbor, and gratefully acknowledges their hospitality. This work was supported in part by NASA through grants NNX12AC98G, NNX15AP39G, and Hubble Theory Grants HST-AR-13261.01-A and HST-AR-14315.001-A. The simulations were run on the NASA Pleiades supercomputer under allocation SMD-15-6514. The active particle framework, upon which our AGN implementation is based, was developed by Nathan Goldbaum at NCSA, and we thank him for his support. `Enzo` and `yt` are developed by a large number of independent researchers from numerous institutions around the world. Their commitment to open science has helped make this work possible.

REFERENCES

- Babul, A., Sharma, P., & Reynolds, C. S. 2013, *ApJ*, 768, 11
- Balbus, S. A. 2000, *ApJ*, 534, 420
- . 2001, *ApJ*, 562, 909
- Binney, J., & Tabor, G. 1995, *MNRAS*, 276, 663
- Blandford, R. D., & Payne, D. G. 1982, *MNRAS*, 199, 883
- Blandford, R. D., & Znajek, R. L. 1977, *MNRAS*, 179, 433
- Bondi, H. 1952, *MNRAS*, 112, 195
- Booth, C. M., & Schaye, J. 2009, *MNRAS*, 398, 53
- Bryan, G. L., Norman, M. L., O’Shea, B. W., et al. 2014, *ApJS*, 211, 19
- Carilli, C. L., & Taylor, G. B. 2002, *ARA&A*, 40, 319
- Cavagnolo, K. W., Donahue, M., Voit, G. M., & Sun, M. 2008, *ApJ*, 683, L107
- . 2009, *ApJS*, 182, 12
- Churazov, E., Brügggen, M., Kaiser, C. R., Böhringer, H., & Forman, W. 2001, *ApJ*, 554, 261
- Churazov, E., Sazonov, S., Sunyaev, R., et al. 2005, *MNRAS*, 363, L91
- Colella, P., & Woodward, P. R. 1984, *Journal of Computational Physics*, 54, 174
- Di Matteo, T., Colberg, J., Springel, V., Hernquist, L., & Sijacki, D. 2008, *ApJ*, 676, 33
- Dubois, Y., Devriendt, J., Slyz, A., & Silk, J. 2009, *MNRAS*, 399, L49
- Dubois, Y., Devriendt, J., Slyz, A., & Teyssier, R. 2012, *MNRAS*, 420, 2662
- Dunn, R. J. H., Fabian, A. C., & Sanders, J. S. 2006, *MNRAS*, 366, 758
- Dursi, L. J., & Pfrommer, C. 2008, *ApJ*, 677, 993
- Edge, A. C. 2001, *MNRAS*, 328, 762
- Ferrarese, L., & Merritt, D. 2000, *ApJ*, 539, L9
- Fryxell, B., Olson, K., Ricker, P., et al. 2000, *ApJS*, 131, 273
- Gaspari, M., Brighenti, F., D’Ercole, A., & Melioli, C. 2011a, *MNRAS*, 415, 1549
- Gaspari, M., Melioli, C., Brighenti, F., & D’Ercole, A. 2011b, *MNRAS*, 411, 349
- Gaspari, M., Ruzskowski, M., & Sharma, P. 2012, *ApJ*, 746, 94
- Hahn, O., Martizzi, D., Wu, H.-Y., et al. 2015, *ArXiv e-prints*, arXiv:1509.04289
- Hopkins, P. F., & Hernquist, L. 2006, *ApJS*, 166, 1
- Kauffmann, G., Heckman, T. M., Tremonti, C., et al. 2003, *MNRAS*, 346, 1055
- Khalatyan, A., Cattaneo, A., Schramm, M., et al. 2008, *MNRAS*, 387, 13
- Kirkpatrick, C. C., & McNamara, B. R. 2015, *MNRAS*, 452, 4361
- Kirkpatrick, C. C., McNamara, B. R., & Cavagnolo, K. W. 2011, *ApJ*, 731, L23
- Li, Y., & Bryan, G. L. 2012, *ApJ*, 747, 26
- . 2014a, *ApJ*, 789, 54
- . 2014b, *ApJ*, 789, 153
- Li, Y., Bryan, G. L., Ruzskowski, M., et al. 2015, *ApJ*, 811, 73
- Loubser, S. I., Babul, A., Hoekstra, H., et al. 2015, *ArXiv e-prints*, arXiv:1511.07884
- Mathews, W. G., Faltenbacher, A., & Brighenti, F. 2006, *ApJ*, 638, 659
- Mathews, W. G., & Guo, F. 2012, *ApJ*, 754, 154
- McCourt, M., Sharma, P., Quataert, E., & Parrish, I. J. 2012, *MNRAS*, 419, 3319
- McDonald, M., Veilleux, S., Rupke, D. S. N., Mushotzky, R., & Reynolds, C. 2011, *ApJ*, 734, 95
- McDonald, M., Stalder, B., Bayliss, M., et al. 2015, *ArXiv e-prints*, arXiv:1508.06283
- McNamara, B. R., & Nulsen, P. E. J. 2007, *ARA&A*, 45, 117
- . 2012, *New Journal of Physics*, 14, 055023
- Meece, G. R., O’Shea, B. W., & Voit, G. M. 2015, *ApJ*, 808, 43
- Merritt, D. 2000, in *Astronomical Society of the Pacific Conference Series*, Vol. 197, *Dynamics of Galaxies: from the Early Universe to the Present*, ed. F. Combes, G. A. Mamon, & V. Charmandaris, 221
- Nagai, D., Kravtsov, A. V., & Vikhlinin, A. 2007, *ApJ*, 668, 1
- Nulsen, P. E. J., & McNamara, B. R. 2013, *Astronomische Nachrichten*, 334, 386
- O’Dea, C. P., Baum, S. A., Privon, G., et al. 2008, *ApJ*, 681, 1035
- O’Dea, K. P., Quillen, A. C., O’Dea, C. P., et al. 2010, *ApJ*, 719, 1619
- Omma, H., Binney, J., Bryan, G., & Slyz, A. 2004, *MNRAS*, 348, 1105
- Parrish, I. J., Quataert, E., & Sharma, P. 2009, *ApJ*, 703, 96
- Peterson, J. R., & Fabian, A. C. 2006, *Phys. Rep.*, 427, 1
- Peterson, J. R., Kahn, S. M., Paerels, F. B. S., et al. 2003, *ApJ*, 590, 207
- Pizzolato, F., & Soker, N. 2005, *ApJ*, 632, 821
- Puchwein, E., Sijacki, D., & Springel, V. 2008, *ApJ*, 687, L53
- Quataert, E. 2008, *ApJ*, 673, 758
- Rasia, E., Borgani, S., Murante, G., et al. 2015, *ApJ*, 813, L17
- Ruzskowski, M., Enßlin, T. A., Brügggen, M., Heinz, S., & Pfrommer, C. 2007, *MNRAS*, 378, 662
- Ruzskowski, M., Lee, D., Brügggen, M., Parrish, I., & Oh, S. P. 2011, *ApJ*, 740, 81
- Schure, K. M., Kosenko, D., Kaastra, J. S., Keppens, R., & Vink, J. 2009, *A&A*, 508, 751
- Sharma, P., McCourt, M., Quataert, E., & Parrish, I. J. 2012, *MNRAS*, 420, 3174
- Sijacki, D., Springel, V., Di Matteo, T., & Hernquist, L. 2007, *MNRAS*, 380, 877
- Skory, S., Hallman, E., Burns, J. O., et al. 2013, *ApJ*, 763, 38
- Smith, B., O’Shea, B. W., Voit, G. M., Ventimiglia, D., & Skillman, S. W. 2013, *ApJ*, 778, 152
- Springel, V., Di Matteo, T., & Hernquist, L. 2005a, *MNRAS*, 361, 776
- Springel, V., White, S. D. M., Jenkins, A., et al. 2005b, *Nature*, 435, 629
- Steinborn, L. K., Dolag, K., Hirschmann, M., Prieto, M. A., & Remus, R.-S. 2015, *MNRAS*, 448, 1504
- Stone, J. M., & Norman, M. L. 1992, *ApJS*, 80, 753
- Sutter, P. M., Yang, H.-Y. K., Ricker, P. M., Foreman, G., & Pugmire, D. 2012, *MNRAS*, 419, 2293
- Turk, M. J., Smith, B. D., Oishi, J. S., et al. 2011, *ApJS*, 192, 9
- Vernaleo, J. C., & Reynolds, C. S. 2006, *ApJ*, 645, 83
- Vogelsberger, M., Genel, S., Sijacki, D., et al. 2013, *MNRAS*, 436, 3031
- Vogelsberger, M., Genel, S., Springel, V., et al. 2014, *MNRAS*, 444, 1518
- Voit, G. M. 2005, *Reviews of Modern Physics*, 77, 207
- Voit, G. M., & Bryan, G. L. 2001, *Nature*, 414, 425
- Voit, G. M., Bryan, G. L., Balogh, M. L., & Bower, R. G. 2002, *ApJ*, 576, 601
- Voit, G. M., Cavagnolo, K. W., Donahue, M., et al. 2008, *ApJ*, 681, L5
- Voit, G. M., & Donahue, M. 2015, *ApJ*, 799, L1
- Voit, G. M., Donahue, M., Bryan, G. L., & McDonald, M. 2015, *Nature*, 519, 203
- Wagh, B., Sharma, P., & McCourt, M. 2014, *MNRAS*, 439, 2822
- Wilman, R. J., Edge, A. C., & Johnstone, R. M. 2005, *MNRAS*, 359, 755
- Wurster, J., & Thacker, R. J. 2013, *MNRAS*, 431, 2513
- Yang, H.-Y. K., & Reynolds, C. S. 2015, *ArXiv e-prints*, arXiv:1512.05796
- Yang, H.-Y. K., Sutter, P. M., & Ricker, P. M. 2012, *MNRAS*, 427, 1614